Ionics (2018) 24:3291–3297
https://doi.org/10.1007/s11581-018-2640-1

SHORT COMMUNICATION

Investigation of charge recombination lifetime in γ-WO_3 films modified with Ag^0 and Pt^0 nanoparticles and its influence on photocurrent density

M. J. S. Costa[1] · G. S. Costa[1] · A. E. B. Lima[1] · G. E. Luz Jr[1] · E. Longo[2] · L. S. Cavalcante[1] · R. S. Santos[1]

Received: 22 April 2018 / Revised: 31 May 2018 / Accepted: 25 June 2018 / Published online: 6 July 2018

Abstract

In this communication, we report the growth of pure gamma-phase tungsten oxide (γ-WO_3) films on a conducting substrate (fluorine-doped tin oxide), followed by heat treatment at 500 °C for 2 h, and finally modification with either silver (Ag^0) or platinum (Pt^0) metallic nanoparticles. These γ-WO_3 thin films can be obtained from a tungsten citrate solution by a drop-coating method, and their surfaces are modified with Ag^0 and Pt^0 nanoparticles by photoreduction. X-ray diffraction analysis indicates that all the thin films have a monoclinic structure. Field emission-scanning electron microscopy analysis reveals large and fine grains for pure γ-WO_3 film and modified WO_3 films, respectively, with an average grain size of ~ 48 nm and thickness of ~ 986 nm. Finally, an enhancement in photoelectrochemical performance by a factor of ~ 2.5 is noted to modified γ-WO_3 films, which is attributed to superior electron-hole charge recombination lifetime under polychromatic irradiation. It is observed that, even under bias, an exponential reduction in photocurrent intensity is associated with charge recombination instead of mass transport conditions like diffusion.

Keywords γ-WO_3 films · Ag^0/Pt^0 nanoparticles · Recombination lifetime · Transient photocurrent

Introduction

Nowadays, water and energy issues have attracted sustained interest from research groups due to the effects of large population growth in urban centers [1]. Photoelectrochemical water splitting, based on semiconductors supported onto a conducting substrate, is regarded as a potential strategy to solve the energy and environmental problems. Several semiconductor oxides have been used as photoelectrocatalysts for $H_{2(g)}$ and $O_{2(g)}$ evolution reactions [2–4] and for degradation of organic pollutants in wastewater [5]. Among the different oxide semiconductors investigated for electrochemical applications (water splitting, electrochromic materials, photoanodes, catalysis, and photocatalysis), the main ones are TiO_2, WO_3, $CuWO_4$, ZnO, and α-Fe_2O_3 [6–10].

WO_3 crystals can exhibit different crystalline structures. These polymorphs are assigned as alpha (α) for the orthorhombic structure with space group *Pmnb* (formed at temperatures from 330 to 740 °C), beta (β) for the tetragonal structure with space group *P4/nmm* (formed at temperatures above 740 °C), gamma (γ) for the monoclinic structure with space group $P2_1/n$ (formed at temperatures from 17 to 330 °C), and delta (δ) for the triclinic structure with space group $P\bar{1}$ (formed at temperatures from − 50 to 17 °C) [11–13]. Therefore, the most common structure is monoclinic γ-WO_3. The γ-WO_3 crystal is an *n*-type oxide semiconductor with an indirect optical band gap energy (E_{BG}) varying from 2.6 to 2.8 eV [14], which allows visible-light harvesting and makes it a good photocatalyst [15].

In addition, WO_3 films are among the most-studied photoanode materials in photoelectrochemical cells (PECs) due to good electrochemical performance in acidic aqueous media, low cost, nontoxicity, facile synthesis, and efficient electron transport properties [16, 17]. To improve the photocatalytic performance of WO_3 thin films for PEC-based water splitting, it is necessary to reduce the electron-hole recombination rate [18]. Additionally, photoelectrocatalysis performance can be improved by modifying the surface of WO_3 films with metal nanoparticles [19].

In general, the photoelectrocatalysis process occurs when a semiconductor material in the form of a film is irradiated with a light source providing energy equal to or higher than its band gap energy. This results in promotion of an electron from the

✉ L. S. Cavalcante
laeciosc@bol.com.br

[1] PPGQ-GERATEC, Universidade Estadual do Piauí, Rua: João Cabral, N. 2231, P.O. Box 381, Teresina, PI 64002-150, Brazil

[2] CDMF-Universidade Estadual Paulista, P.O. Box 355, Araraquara, SP 14801-907, Brazil

filled valence band to the empty conduction band (e^-_{CB}) and generation of a positively charged hole (h^+_{VB}) [20]. Using a semiconductor photocatalyst as a photoanode, it is possible to apply a bias potential to the cell aiming to minimize the charge recombination effects. This photoanode polarization favors the flow of photoinduced electrons e^-_{CB} through an external electrical circuit, which normally increases the efficiency of the photocatalytic process [21].

Usually, reports in the literature focus on bias conditions and metal surface modification as strategies to reduce the electron-hole charge recombination. However, there have been no systematic studies to evaluate these approaches. Therefore, this communication aims to evaluate the importance of WO_3 films modified with Ag^0 and Pt^0 nanoparticles in increasing the charge recombination lifetime. Besides, it was shown by transient photocurrent measurements that a reduction in the photocurrent signal is really associated with electron-hole charge recombination and not diffusional mass transport.

Experimental details

The γ-WO_3 films were deposited by a simple drop-casting method from an aqueous solution of tungsten citrate (9.3115×10^{-5} mol L^{-1}), which was synthesized by a modified complex polymerization (CP) method [22], and annealed at 500 °C for 2 h (heating rate of 2 °C/min) in a muffle furnace to remove organic compounds from the precursor solution. Then, the metallic nanoparticle deposition was performed by a photoreduction method as follows. Firstly, aqueous solutions of 1.0 mmol L^{-1} silver nitrate ($AgNO_3$; 99% purity; Sigma-Aldrich) and 1.0 mmol L^{-1} hexachloroplatinic acid hexahydrate ($H_2Cl_6Pt{\cdot}6H_2O$, 37.5% purity; Sigma-Aldrich) were prepared to provide the sources for Ag^+ and Pt^{4+} ions, respectively. Secondly, these γ-WO_3 films were immersed in the aqueous solution containing either the Ag^+ or Pt^{4+} ions for 10 s. Finally, these γ-WO_3 films were placed under ultraviolet (UV) light irradiation, in a closed box configured with three STARLUX 20 W lamps, for a period of 5 min and washed several times with deionized water to ensure complete removal of unreduced precursor metals.

The structure, morphology, and photoelectrochemical properties were investigated by different characterization techniques. The crystal phase and size of these films were analyzed with an X-ray diffractometer (XRD) and the shape and thickness with a scanning electron microscopy (SEM). XRD patterns of the films were obtained using a LabX XRD-6000 diffractometer (Shimadzu, Japan) with Cu-Kα radiation (wavelength λ = 0.15406 nm) and were compared to the data from the Inorganic Crystal Structure Database (ICSD). The morphology of the samples was analyzed by field emission-scanning electron microscopy (FE-SEM) in an FEI Quanta (FEG 250 model, Philips©) operated at 20 kV and a magnification of × 200,000.

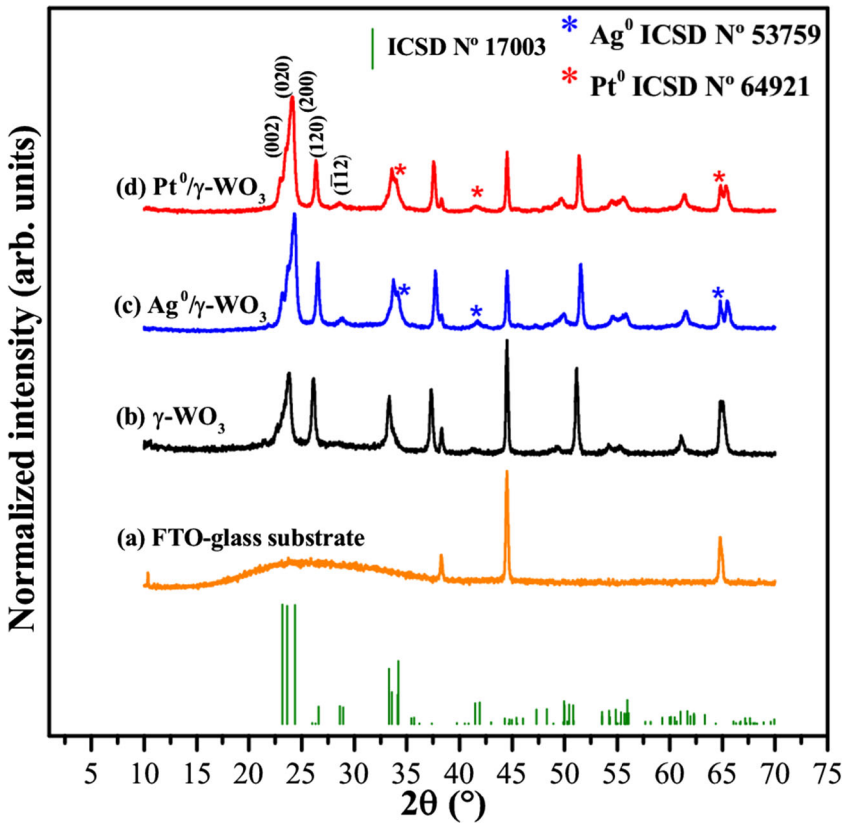

Fig. 1 XRD patterns of (**a**) FTO glass substrate, (**b**) pure γ-WO_3 film, (**c**) Ag^0/γ-WO_3 film modified, and (**d**) Pt^0/γ-WO_3 film modified prepared by drop-casting method annealing at 500 °C for 2 h. Vertical lines indicate plane position and intensity of γ-WO_3 phase with monoclinic structure related to ICSD card no. 17003

Photoelectrochemical properties were investigated using an electrochemical cell equipped with an optical glass window (100% transmittance for $\lambda > 360$ nm). These studies were performed in a three-electrode system configuration, and 0.1 mol L^{-1} Na_2SO_4 (pH 5.6) was utilized as a support electrolyte. The working electrodes were the γ-WO_3, Ag^0/γ-WO_3, and Pt^0/γ-WO_3 films (ca. geometrical area of 1 cm^2); a Pt^0 wire was the counter electrode; and Ag/AgCl (in a 3.0 mol L^{-1} potassium chloride saturated aqueous solution) was used as the reference electrode (in a Luggin capillary). The measurements were performed with a galvanostat/potentiostat (Autolab PGSTAT 302-N) in both the absence of light (dark) and under polychromatic irradiation. To irradiate the γ-WO_3 films, a metallic vapor discharge lamp (HQI-TS NDL) with a nominal power of 150 W was utilized. Photocurrent was measured using linear sweep voltammetry (LSV), with the data recorded in the anodic potential range of 0.1–1.2 V at a scan rate of 5.0 mV s^{-1}, with chopped irradiation at a frequency of 0.2 Hz. Chronoamperometric curves were collected under dark or light conditions with the electrodes polarized at three potentials, 0.3, 0.5, and 0.7 V (vs. Ag/AgCl). From the photoresponse, it was possible to calculate the recombination lifetime from the time constant (τ) obtained from Eq. (1), which describes the kinetics of the transient currents as follows:

$$R = \exp\left(-{}^{t}/_{\tau}\right), \quad (1)$$

where the ratio R is $\frac{J_t - J_{st}}{J_{in} - J_{st}}$, J_t is the photocurrent at time t, J_{st} is the steady-state photocurrent, and J_{in} is the photocurrent at the initial time [23, 24].

Results and discussion

Figures 1(a–d) shows the XRD patterns of a fluorine-doped tin oxide glass substrate (FTO glass substrate), a γ-WO_3 film, a Ag^0/γ-WO_3 film, and a Pt^0/γ-WO_3 film, respectively.

As can be observed in Fig. 1(a), the FTO glass substrate exhibits an amorphous halo from 15° to 35° related to glass (SiO_2) and a crystalline pattern with 3 peaks corresponding to the conductive layer of the SnO_2:F phase. Moreover, it can be noted from Fig. 1(b–d) that all the other XRD peaks from the pure and γ-WO_3 films are related to the monoclinic structure in good concordance with ICSD 17003 [25]. Based on this crystallographic information file (CIF), gamma (γ)-WO_3 is the most stable crystal phase at room temperature [26]. In the XRD patterns for all the films, the (002), (020), and (200) diffraction peaks are the most intense. Moreover, these XRD peaks were overlapped, suggesting that the films are thin and composed of γ-WO_3 nanoparticles. When the γ-WO_3 films were annealed at 500 °C for 2 h, there occurred a partial preferential growth of the (120) diffraction plane, while the ($\bar{1}$ 12) plane almost disappeared (Fig. 1(b)). Peaks at the diffraction angle (2θ) equal to

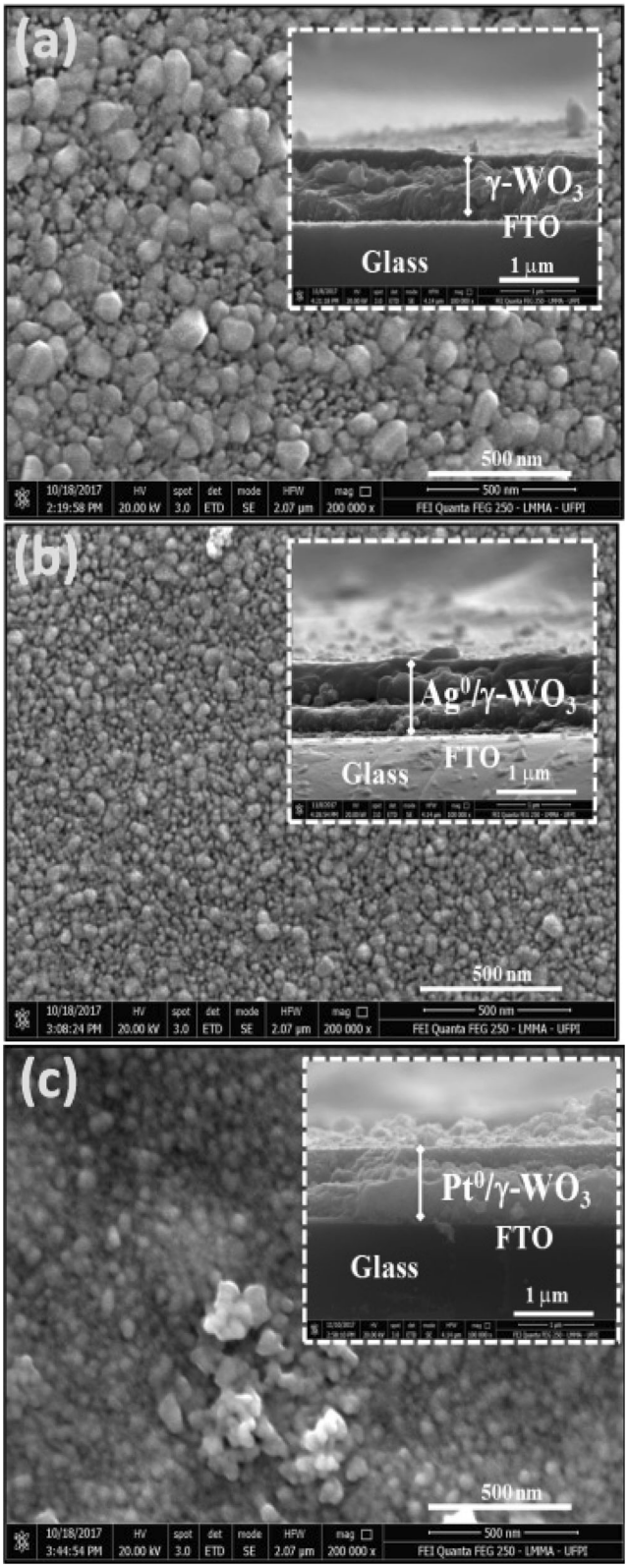

Fig. 2 FE-SEM images of the (**a**) pure γ-WO_3 film, (**b**) Ag^0/γ-WO_3 film, and (**c**) Pt^0/γ-WO_3 film. Inset shows FEG-SEM images of the WO_3 film cross section

38.28°, 44.45°, and 64.80°, attributed to FTO glass, have been observed in all film samples. Also, the diffraction peaks for the body-centered cubic structure of Ag^0 and Pt^0 nanoparticles on the γ-WO_3 films were detected, according to ICSD 53759 [27] and ICSD 64921 [28] (Fig. 1(c, d)), respectively.

Figure 2(a–c) illustrate the FE-SEM images of the γ-WO_3 film, Ag^0/γ-WO_3 film, and Pt^0/γ-WO_3 film all deposited on FTO glass substrates, respectively.

As can be observed in Fig. 2(a), the FE-SEM images of the γ-WO_3 film heat-treated at 500 °C for 2 h exhibited grains with irregular shapes with an average size of 52 ± 5 nm, which can be attributed to the high crystallization rate, and an average thickness of 936 ± 25 nm. Figure 2(b) shows an FE-SEM image of a Ag^0/γ-WO_3 film with a homogeneous grain shape (average grain size of 46 ± 5 nm, which can be attributed to the high crystallization rate, and an average thickness of 1004 ± 25 nm) that can be promoted by incorporation of Ag^0 nanoparticles on the surface of the γ-WO_3 film that causes an inhibition of grain growth in this modified γ-WO_3 film. However, as can be noted in Fig. 2(c), the FE-SEM images indicate that inhomogeneous and nonuniform microstructures are formed with large grains when Pt^0 nanoparticles are added to the γ-WO_3 film (with average size of 45 ± 5 nm, which can be associated to the high crystallization rate, and an average thickness of 1018 ± 25 nm). Therefore, an irregular grain growth mechanism is dominant when Pt^0 nanoparticles are incorporated in the modified γ-WO_3 film. This behavior can be due to Pt^{4+} ions exhibiting a different mobility and by the transformation from Pt^{4+} ions to Pt^0 nanoparticles on the surface of the γ-WO_3 film when exposed to UV light [29].

Figure 3 shows linear anodic sweep voltammograms of supported γ-WO_3 films. In the absence of light (dark), the photocurrent density is almost zero.

As can be observed in Fig. 3, the Ag^0 or Pt^0 nanoparticles on the surface of the γ-WO_3 film lead to a significant improvement in the photocurrent density by almost 2.5 times. At 1.2 V vs. Ag/AgCl (1.73 vs. a reversible hydrogen electrode (RHE)), the irradiated curves reached 200 and 250 μA cm^{-2} for the Ag^0/γ-WO_3 film and Pt^0/γ-WO_3 film, respectively. Initially, the photocurrent response in an *n*-type semiconductor results from an electron-hole (e^-_{CB}/h^+_{VB}) charge separation process under light irradiation with $h\nu \geq E_{BG}$ (where *h* is Planck's constant and *ν* is the photon's frequency). The photogenerated electron can be transferred through the crystallites that constitute the film, if the reaction kinetics of the hole with any species present in solution is faster than the process of electron-hole recombination [30]. However, in a photoelectrochemical system, the electron can reach the conductive substrate and then be collected by the external circuit [31, 32]. Therefore, the increase of photocurrent in both modified films is probably due to the interaction of the semiconductor with the metal nanoparticles. According to the literature [33], the enhancement of photoelectrochemical performance by using a film modified by metal nanoparticles can occur from the surface plasmon resonance (SPR) effect. Consequently, the current increase happens because the metal nanoparticles act as electron traps, scattering or absorbing at the center of the visible light spectrum.

To obtain the electron-hole recombination lifetimes for the photoelectrodes, current-time curves, following the

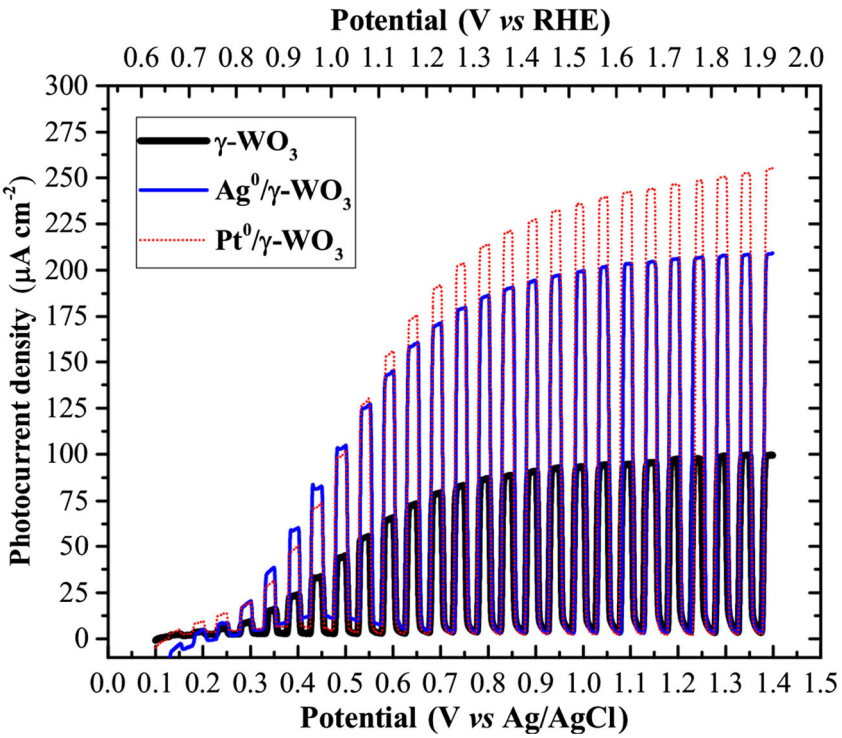

Fig. 3 Linear sweep voltammetry curves of γ-WO_3, Ag^0/γ-WO_3, and Pt^0/γ-WO_3 films illuminated with chopped visible light in an 0.1 mol L^{-1} Na_2SO_4 aqueous solution

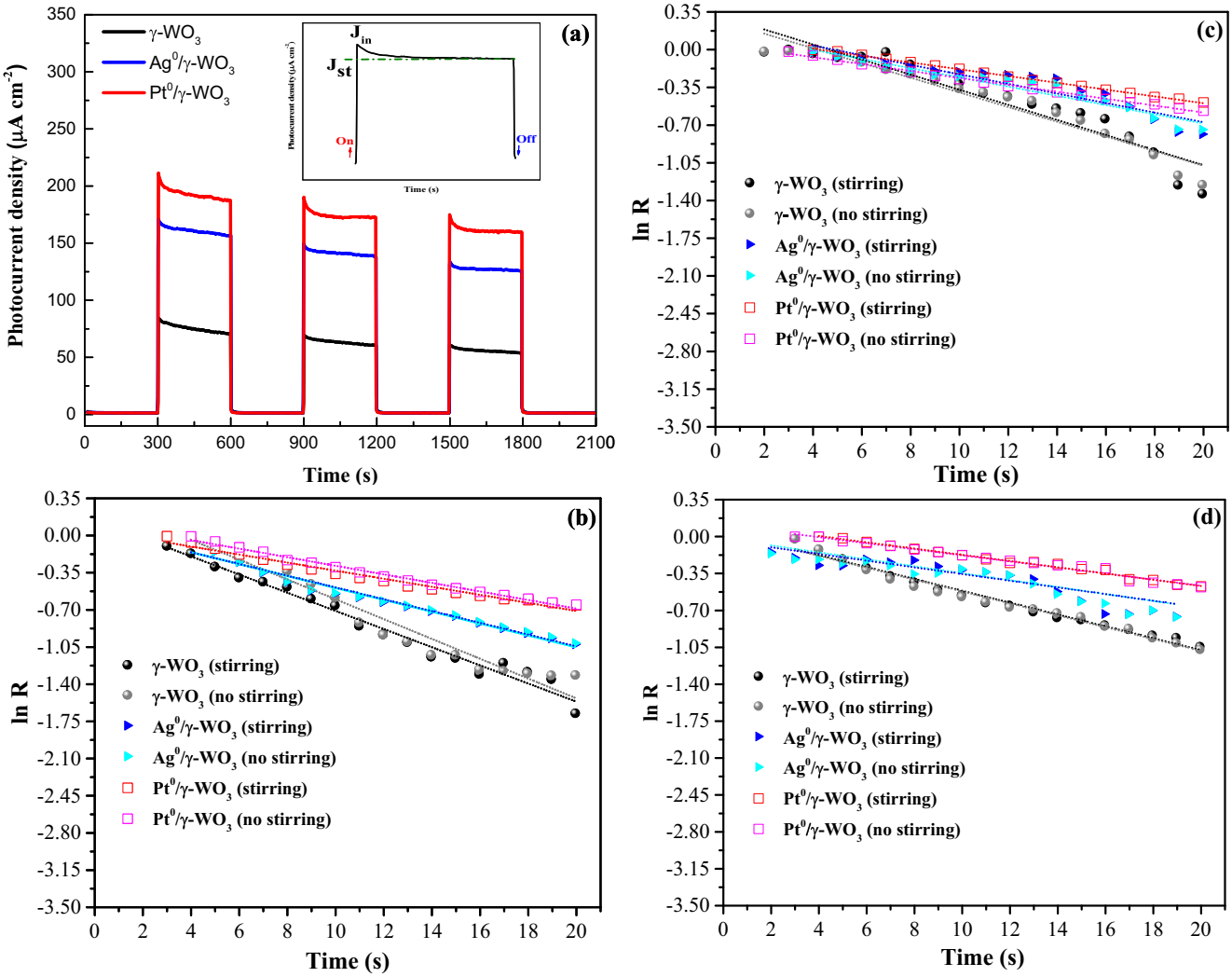

Fig. 4 (**a**) Photocurrent density-time (*j-t*) curves of the annealed films measured under illumination with chopped 300 s light on/off at 0.7 V vs. Ag/AgCl and normalized plot of current-time dependence for γ-WO_3 films, Ag/γ-WO_3 film, and Pt/γ-WO_3 film at (**b**) 0.3 V, (**c**) 0.5 V, and (**d**) 0.7 V

schematic representation in inset Fig. 4(a), were analyzed using Eq. (1). The equation (1) shows that the kinetics of the transient photocurrent can be obtained from a ln R vs. time plot as shown in Fig. 4(b–d) for pure γ-WO_3 film, Ag^0/γ-WO_3 modified film, and Pt^0/γ-WO_3 modified film, respectively, for three applied biases (0.3, 0.5, and 0.7 V) and under varying charge mass transport conditions (stirring and no stirring).

As can be noted in Fig. 4(a), an initial anodic photocurrent spike $J_{(i)}$ indicates the injection of electrons caused by the formation of the electron-hole pairs, i.e., charge separation process. Holes move towards the semiconductor surface where they are reduced by the species in the electrolyte, and electrons are trapped by the Ag^0 and Pt^0 nanoparticles and transported to the back contact to be collected by the external circuit. Afterwards, the photocurrent decreases with time until

Table 1 Photocurrent transient stirring and no stirring with different potential for pure γ-WO_3 film, Ag^0/γ-WO_3 film, and Pt^0/γ-WO_3 film, respectively

Samples	Recombination lifetime (s)					
	γ-WO_3 film		Ag^0/γ-WO_3 film		Pt^0/γ-WO_3 film	
Potential (V)	Stirring	No stirring	Stirring	No stirring	Stirring	No stirring
0.3	11 ± 2	11 ± 1	18 ± 1	18 ± 1	26 ± 2	25 ± 2
0.5	14 ± 1	14 ± 1	22 ± 1	23 ± 2	31 ± 2	31 ± 1
0.7	18 ± 2	18 ± 1	30 ± 2	31 ± 2	34 ± 2	35 ± 3

it reaches a steady-state photocurrent density, $J_{(st)}$. This indicates the occurrence of the charge recombination process. In Fig. 4(b–d), the slope of the plot provides τ, which is related to the charge recombination lifetime in each electrode. The τ value for the pure γ-WO_3 film is smaller than the modified Ag^0/Pt^0/γ-WO_3 films, due to the absence of trapping resulting in slight recombination of photogenerated charges, as displayed in Table 1.

As can be noticed in Table 1, these recombination lifetime values are similar under both charge mass transport conditions. This means that convection or diffusion in the system does not alter the recombination lifetime even under extreme bias conditions. An increase in the photocurrent only occurred in the modified films. Therefore, the photoelectrochemical properties were enhanced in the γ-WO_3 films modified with Ag^0 and Pt^0 nanoparticles.

Conclusions

In summary, this study revealed that pure γ-WO_3 film and γ-WO_3 films modified with Ag^0 or Pt^0 nanoparticles can be synthesized by drop-casting and photoreduction methods. XRD patterns indicated that the pure and modified γ-WO_3 films exhibited monoclinic structures, and FE-SEM images showed the presence of grains with an irregular shape. Photoelectrochemical studies showed an increase in photoelectrochemical performance of about 2.5 times for γ-WO_3 films modified with Ag^0 and Pt^0 nanoparticles. The best response was registered for films modified by Pt^0 nanoparticles. This improvement in the photocurrent was attributed to better charge separation induced by metal nanoparticles, because these particles act as electrons traps. The results were not altered under different conditions of charge mass transport, but the bias potential utilized improved the current and the recombination time. Thus, γ-WO_3 films modified with Ag^0 or Pt^0 nanoparticles are very promising semiconductor oxides for PEC-based photoelectrocatalytic applications.

Funding information This study is financially supported by the Brazilian research financing institutions: CNPq (479644/2012-8 and 304531/2013-8), FAPESP (2013/07296-2), and CAPES.

References

1. Mao J, Zhang Q, Li P, Zhang L, Zhang W (2018) Geometric architecture design of ternary composites based on dispersive WO_3 nanowires for enhanced visible-light-driven activity of refractory pollutant degradation. Chem Eng J 334:2568–2578
2. Tanaka A, Hashimoto K, Kominami H (2014) Visible-light-induced hydrogen and oxygen formation over Pt/Au/WO_3 photocatalyst utilizing two types of photoabsorption due to surface plasmon resonance and band-gap excitation. J Am Chem Soc 136(2):586–589
3. Ji X, Ma M, Ge R, Ren X, Wang H, Liu J, Liu Z, Asiri AM, Sun X (2017) WO_3 nanoarray: an efficient electrochemical oxygen evolution catalyst electrode operating in alkaline solution. Inorg Chem 56(24):14743–14746
4. Jeon B, Kim A, Lee Y-A, Seo H, Kim YK (2017) A spontaneous change in the oxidation states of Pd/WO_3 toward an active phase during catalytic cycles of CO oxidation. Surf Sci 665:43–50
5. Garcia-Segura S, Brillas E (2017) Applied photoelectrocatalysis on the degradation of organic pollutants in wastewaters. J Photochem Photobiol C Photochem Rev 31:1–35
6. Tang J, Durrant JR, Klug DR (2008) Mechanism of photocatalytic water splitting in TiO_2. Reaction of water with photoholes, importance of charge carrier dynamics, and evidence for four-hole chemistry. J Am Chem Soc 130:13885–13891
7. Bucha VR, Chawla AK, Rawal SK (2016) Review on electrochromic property for WO_3 thin films using different deposition techniques. Mater Today 3:1429–1437
8. Lima AEB, Costa MJS, Santos RS, Batista NC, Cavalcante LS, Longo E, Luz GE Jr (2017) Facile preparation of $CuWO_4$ porous films and their photoelectrochemical properties. Electrochim Acta 256:139–145
9. Nikoofar K, Haghighi M, Lashanizadegan M, Ahmadvand Z (2015) ZnO nanorods: efficient and reusable catalysts for the synthesis of substituted imidazoles in water. J Taibah Univ Sci 9:570–578
10. Mishra M, Chun D-M (2015) α-Fe_2O_3 as a photocatalytic material: a review. Appl Catal A Gen 498:126–141
11. Salje E, Viswanatha K (1975) Physical properties and phase transitions in WO_3. Acta Cryst A31:356–359
12. Salje E (1977) The orthorhombic phase of WO_3. Acta Cryst B33: 574–577
13. Souza Filho AG, Filho JM, Freire VN, Ayala AP, Sasaki JM, Freire PTC, Melo FEA, Julião JF, Gomes UU (2001) Phase transition in WO_3 microcrystals obtained by sintering process. J Raman Spectrosc 32:695–699
14. Go GH, Shinde PS, Doh CH, Lee WJ (2016) PVP-assisted synthesis of nanostructured transparent WO_3 thin films for photoelectrochemical water splitting. Mater Des 90:1005–1009
15. Umukoro EH, Peleyeju MG, Ngila JC, Arotiba OA (2017) Towards wastewater treatment: photo-assisted electrochemical degradation of nitrophenol and orange II dye at a tungsten trioxide-exfoliated graphite composite electrode. Chem Eng J 369:8–18
16. Shinde PA, Lokhande VC, Chodankar NR, Ji T, Kim JH, Lokhande CD (2016) Enhanced electrochemical performance of monoclinic WO_3 thin films with redox additive aqueous electrolyte. J Colloid Interface Sci 483:261–267
17. Zhang J, Ma H, Liu Z (2017) Highly efficient photocatalyst based on all oxides WO_3/Cu_2O heterojunction for photoelectrochemical water splitting. Appl Catal B Environ 201:84–91
18. Liu Z, Wu J, Zhang J (2016) Quantum dots and plasmonic Ag decorated WO_3 nanorod photoanodes with enhanced photoelectrochemical performances. Int J Hydrog Energy 41(45): 20529–20535
19. Ding J, Zhang L, Liu Q, Dai WL, Guan G (2017) Synergistic effects of electronic structure of WO_3 nanorods with the dominant {001} exposed facets combined with silver size-dependent on the visible-light photocatalytic activity. Appl Catal B Environ 203:335–342
20. Oliveira HG, Ferreira LH, Bertazzoli R, Longo C (2015) Remediation of 17-α-ethinylestradiol aqueous solution by photocatalysis and electrochemically assisted photocatalysis using TiO_2 and TiO_2/WO_3 electrodes irradiated by a solar simulator. Water Res 72:305–314
21. Garcia-Segura S, O'Neal Tugaoen H, Hristovski K, Westerhoff P (2018) Photon flux influence on photoelectrochemical water treatment. Electrochem Commun 87:63–65

22. Cavalcante LS, Sczancoski JC, Albarici VC, Matos JME, Varela JA (2008) Synthesis, characterization, structural refinement and optical absorption behavior of $PbWO_4$ powders. Mater Sci Eng B 150:18–25
23. Dholam R, Patel N, Santini A, Miotello A (2010) Efficient indium tin oxide/Cr-doped-TiO_2 multilayer thin films for H_2 production by photocatalytic water-splitting. Int J Hydrog Energy 35:9581–9590
24. Spadavecchia F, Ardizzone S, Cappelletti G, Falciola L, Ceotto M, Lotti D (2013) Investigation and optimization of photocurrent transient measurements on nano-TiO_2. J Appl Electrochem 43:217–225
25. S.Tanisaki (1960) Crystal structure of monoclinic tungsten trioxide at room temperature. J Phys Soc Jpn 15(4):573–581
26. Zheng JY, Song G, Hong J, Thanh KV, Pawar AU, Kim DY, Kim CW, Haider Z, Kang YS (2014) Facile fabrication of WO_3 nanoplates thin films with dominant crystal facet of (002) for water splitting. Cryst Growth Des 14:6057–6066
27. Vegard L (1916) IX, The structure of silver crystals. Philos Mag Ser 31(181):83–87
28. Kahler H (1921) The crystalline structures of sputtered and evaporated metallic films. Phys Rev 18(3):210–217
29. Qu Y, Gao Y, Kong F, Zhang S, Du L, Yin G (2013) Pt-rGO-TiO_2 nanocomposite by UV photoreduction method as promising electrocatalyst for methanol oxidation. Int J Hydrog Energy 38: 12310–12317
30. Yoon H, Mali MG, Kim M, Al-Deyab SS, Yoon SS (2015) Electrostatic spray deposition of transparent tungsten oxide thin-film photoanodes for solar water splitting. Catal Today 260:89–94
31. Soedergren S, Hagfeldt A, Olsson J, Lindquist SE (1994) Theoretical models for the action spectrum and the current-voltage characteristics of microporous semiconductor films in photoelectrochemical cells. J Phys Chem 98:5552–5556
32. Hagfeldt A, Grätzel M (1995) Light-induced redox reactions in nanocrystalline systems. Chem Rev 95:49–68
33. Valenti M, Dolat D, Biskos G, Schmidt-Ott A, Smith WA (2015) Enhancement of the photoelectrochemical performance of $CuWO_4$ thin films for solar water splitting by plasmonic nanoparticle functionalization. J Phys Chem C 119:2096–2104